EURASIAN PHYSICAL TECHNICAL JOURNAL

2025, Volume 22, No. 2 (52)

https://doi.org/10.31489/2025N2/42-53

Received: 02/12/2025 Revised: 10/04/2025 Accepted: 27/05/2025 Published online: 30/06/2025

Research Article

UDC 537.311.33; 620.82

ENHANCED EFFICIENCY OF DYE-SENSITIZED SOLAR CELLS USING ZNO NANOPARTICLE DOPING CU FROM PINEAPPLE PEEL EXTRACT WITH MODIFIED NATURAL DYE SOLUTION

Rohmawati L.[1*], Ferdianto S.P.[1], Ma'arif M.S.[1], Ardiansyah F.F.[1], Muadhif F.I.[2,3], Setyarsih W.[1], Supardi Z.A.I.[1], Darminto D.[4]

[1] Universitas Negeri Surabaya, Ketintang, Surabaya, Indonesia
[2] Graduated School, Institut Teknologi Bandung, Bandung, Indonesia
[3] Research Center for System Nanotechnology, National Research and Innovation Agency, Tangerang Selatan, Banten, Indonesia
[4] Institut Teknologi Sepuluh Nopember, Keputih, Surabaya, Indonesia

*Corresponding author: lydiarohmawati@unesa.ac.id

Abstract. *Photoanodes and dye solutions are indispensable in the stability and efficiency of Dye-Sensitized Solar Cells' performance. In this study, the photoanode uses a ZnO sample doped with Cu, made using a green synthesis technique with bio-reduction from pineapple skin extract. Meanwhile, using the maceration method, the dye solution is made from mulberry fruit extract and moringa leaves. For Dye-Sensitized Solar Cells applications, ZnO photoanodes doped with 1%, 3%, 5%, and 10% Cu were each depleted on ITO glass and immersed in the dye solution for one day. The results were then tested for electrical conductivity and performance in Dye-Sensitized Solar Cells. Adding Cu doping concentration to the ZnO photoanode can affect the performance of the Dye-Sensitized Solar Cell. In this work, the ZnO sample doped with 5% Cu as a photoanode showed the highest efficiency at 1.67% with an electron lifetime of 12 ms, compared to the photoanode without Cu doping or with Cu doping at concentrations of 1%, 3%, and 10%. Thus, Cu-doped ZnO nanoparticles and dye solutions from natural materials can be further developed for Dye-Sensitized Solar Cells applications.*

Keywords: Dye-Sensitized Solar Cells, ZnO nanoparticles, Cu Doping, Dye Solution, Green synthesis.

1. Introduction

Dye-sensitized solar Cells (DSSC) are third-procreation solar cells with low outlay, simplicity, and high efficiency. These advantages make DSSCs attractive to industry because they offer renewable energy solutions with low pollution levels and are environmentally friendly. However, DSSCs have weaknesses in the type of dye solution, namely ruthenium, where the availability in nature is minimal (0.0001 ppm) [1] so it is not practical for large-scale use even in the long term, although this material has a high energy conversion value, reaching 13%. It is a consideration for large-scale DSSC applications, so an alternative to using dye solutions from natural materials is needed.

Natural pigments such as chlorophyll, carotenoids, anthocyanins, lutein, rutin, and betalains extracted from various parts of plants, including flowers, fruits, and leaves, can be used as sensitizers in DSSC [2]. Black mulberry fruit (*Morus nigra L.*) and moringa leaves (*Moringa oleifera*) are rich in anthocyanins and chlorophyll. Black mulberry fruit contains anthocyanin pigments of 570.10 ± 77.09 mg/100 g [3] and a light absorption peak of 550 nm. That absorption is similar to ruthenium's, even showing a power conversion

efficiency of 1.3% [4]. Likewise, Moringa leaves have a chlorophyll content of 10.19-16.51 mg/liter [5] and a peak light absorption of 665 nm [6].

Not only dye solutions but also semiconductor materials, such as photoelectrodes, also affect the efficiency of DSSC performance. One of these materials is ZnO, which features a bandgap of 3.37 eV with an exciton binding energy of 60 meV [7]. This value is higher than other metal oxides, making ZnO efficient for various applications, including antibacterial medication, dye removal, gas sensors, and photoanodes for water splitting [8]. Compared to TiO_2, ZnO can absorb energy at a larger wavelength and higher electron mobility [9]. However, using ZnO on a large scale still needs improvement, given its low efficiency in visible light and the rapid recombination of electron-hole pairs [10]. In addition, ZnO tends to form an agglomeration layer on the surface [11]. Therefore, doping with cationic elements such as Cu is needed to enhance the ZnO sample's ability to absorb visible light, reduce charge pair recombination, and increase electron mobility [11].

Cu metal has an ionic radius similar to Zn, allowing Cu to enter the ZnO matrix and change its optical properties [12]. Several methods, including co-precipitation, have successfully synthesized Cu-doped ZnO nanoparticles for DSSC photoanode applications [8], Layered Double Hydroxide (LDH) [13], sol-gel [14], hydrothermal [11], adsorption, and successive ionic layer reaction (SILAR) [2]. Nevertheless, these methods generally use special and toxic chemicals as intermediaries to reduce the size and stabilize nanoparticles, so they are not environmentally friendly. The use of green synthesis pathways is very relevant to in the manufacture of nanoparticles today because the toxicity level of the synthesis process can be reduced so much that the negative impact on the environment [15] and does not even require high temperatures and excessive energy and is environmentally friendly [16]. Khan et al. [17] reported using the green synthesis method to synthesize Cu-doped ZnO from horsetail leaf extract (*Stachytarpheta jamaicensis*). However, the study only focused on antibacterial applications, and the fabrication results still contained Cu ions with a 5 wt% doping composition. In previous studies [18], they successfully synthesized nanoparticles of ZnO through green synthesis using bioreduction from pineapple peel extract. However, that study was only for photocatalyst applications. In contrast, DSSC applications have never been reported, let alone the material used: ZnO nanoparticles doped with Cu, which is manufactured using the green synthesis method.

This research focuses on manufacturing Cu-doped ZnO nanoparticle photoanodes using the green synthesis method from pineapple peel extract with dye solution modification from black mulberry fruit extract and moringa leaves for DSSC applications. Pineapple peel has been considered organic waste, and its utilization can be even better besides being used as animal feed. It should be noted that pineapple peel contains bioactive compounds such as saponins, flavonoids, tannins, anthocyanins, vitamin C, carotenoids, and bromelain enzymes, which can reduce Zinc ions into ZnO nanoparticles [18]. In addition, these compounds can also function as stabilizers in metal solutions by binding to hydroxyls and carboxylates, forming a protective layer around metal particles, preventing aggregation, and even maintaining particle size and distribution [19]. This study was conducted to determine how adding Cu doping to ZnO nanoparticles affects the efficiency and absorption of photon energy in DSSC.

2. Materials and Methods

2.1 Materials

The following are the materials that need to be prepared in this study: Moringa leaves (*Moringa Olivera*), black mulberry fruit (*Morus Nigra L.*), distilled water, ethanol (Merck), $CuSO4.5H_2O$ (Merck), $Zn(CH_3COO)_2.2H_2O$ (Sigma Aldrich), NaOH (Sigma Aldrich), acetic acid (Merck), potassium iodide 0.5 M (Merck), KCl 3 M (Merck), acetonitrile (Emsure), iodine 0.05 M (Emsure), 8B pencil (Staedtler), PVA (Merck), and ITO glass (Sigma Aldrich, 8-12 Ohm-Sq). The equipment used in this study included a mortar pestle, digital balance, dry oven, magnetic bar, hotplate stirrer, beaker glass, petri dish, funnel glass, universal indicator pH, Whatman filter paper, erlenmeyer flask, pipette, spatula, separatory funnel, scotch tape and clamp.

2.2 Preparation of Cu-doped ZnO nanoparticles

Before making ZnO nanoparticles by doping with Cu using the green synthesis method, ZnO nanoparticles were prepared, as described in previous research [18]. Pineapple fruit was separated from the skin to take the pericarp, and the pulp was washed with distilled water. Furthermore, 10 g of pineapple skins were soaked in distilled water and stirred at 75 °C for 1 hour at 350 rpm. The lateness was then left open and

filtered to obtain a yellow filtrate. After that, the solution was mixed with 3 g of Zn $(CH_3COO)_2 \cdot 2H_2O$ and $CuSO_4 \cdot 5H_2O$ at concentrations of 1, 3, 5, and 10 wt.%. It was then added to distilled water and sonicated at 40°C for 90 minutes. The result was blended with 4 g of NaOH and 100 mL of distilled water, then centrifuged at 3000 rpm for 5 minutes. The result was heated at 120°C for 12 hours and then calcined at 500°C for 2 hours.

2.3 Preparation of dye-sensitizer solution

A total of 10 g of Moringa oleifera leaves (*Moringa oleifera*) and black mulberry fruit (*Morus nigra L.*) were crushed with a blender. After that, each ingredient was dissolved with ethanol for the maceration process, left for one day, and then strained using Whatman paper. Black mulberry extract and Moringa leaves were combined in a 1:1 ratio. Then, the natural dye extract was gradually dripped with HCl until a pH of 5 was reached. Furthermore, filtration was carried out, and a dye solution was obtained from a mixture of Moringa leaves and black mulberry fruit.

2.4 Fabrication of DSSC

In the fabrication of DSSC, the first step is to make a photoanode by coating ZnO nanoparticle powder, either without doping or with Cu doping, on the conductive surface of ITO glass using the doctor blade method. Before the coating was carried out, 1.5 g of PVA was dissolved in distilled water and stirred for 30 minutes at 80℃, forming a gel. After that, the gel was mixed with 0.5 g of ZnO, either without or with Cu doping, and then stirred using a mortar and pestle until each formed a paste. Before the paste was applied to the ITO glass surface, it was first cleaned with ethanol. The side of the ITO glass was coated with tape, leaving a 2 cm x 2 cm area open in the middle. The ZnO paste, doped with Cu and without Cu doping, was applied to the middle part that was not covered with tape and then heated on a hot plate at 450 °C for 30 minutes. After that, it was soaked in a dye solution for 24 hours to achieve maximum absorption. The counter electrode in this study was made by referring to previous research [20], specifically by shading an 8B pencil graphite on the ITO conductive glass section until evenly distributed.

Furthermore, 0.8 g potassium iodide was dissolved in 10 ml of acetonitrile to make the electrolyte solution. After that, 0.127 g of iodine was mixed with the liquid until it was homogeneous, and an I^-/I_3^- electrolyte solution was obtained. The DSSC construction process uses a sandwich system with two glass substrates, one serving as the working electrode and the other as the counter electrode. The electrolyte solution of I^-/I_3^- ions is dripped between the two sides of the glass and clamped using a clamping clip

2.5 Characterization

Phase identification of Cu-doped ZnO samples can be determined using the Smartlab Rigaku type X-ray Diffraction (XRD) characterization tool, which works using Bragg-Brentano optical rays with a Cu anode radiation source, 40 kV, 30 mA, and a CuKα wavelength of 1.54 Å with a testing angle of 20-80°. The diffraction pattern of the sample, as determined from the characterization results, was then analyzed qualitatively using Match! Software with the search and match technique. The size of the sample's crystallite could be reckoned using the Debye-Scherrer formula. The surface morphological structure of the sample can be identified using Scanning Electron Microscopy (SEM) characterization, type SU3500, brand Hitachi, with a voltage of 15 kV. SEM of characterization results can measure the sample's grain size distribution using a bar scale as a reference, which is then processed using ImageJ software by considering 150 grains. The absorbance of the sample can be measured using a Hitachi UH-5300 type Ultraviolet-visible spectroscopy (UV-Vis) characterization tool at wavelengths of 400-700 nm. The absorbance data from the characterization can be used to determine its bandgap energy using the Tauc Plot method analysis.

The electrochemical properties of DSSC can be determined through Electrochemical Impedance Spectroscopy (EIS) characterization using Gamry Instruments, equipped with Reference 3000. This characterization provides an impedance response to electrical signals at 0.1 Hz - 10 kHz. Electrical resistance in EIS testing is expressed as impedance, a circuit's ability to withstand the flow of electric current. In the Nyquist graph, the x-axis shows the sample's response data for a given frequency range, specifically the real impedance value ($Z' = Z_{real}$), while the y-axis represents the imaginary impedance ($Z'' = Z_{img}$). The elements that form the equivalent circuit consist of series resistance (R_s), Constant Phase Element (CPE), charge transfer resistance (R_{ct}), and Warburg impedance (W), which are used to determine electrochemical and physical phenomena in the cell. R_{ct} is the difference between the highest and lowest values of the semicircle formed on the graph or can be calculated from the starting point to the end point of the semicircle formation.

The R_s value is known from the lowest point on the graph, which is caused by the presence of electrolytes. On the Bode phase plot graph, the value of the effective mass of an electron in the solar cell system (τ) can be determined according to Equation (1) by knowing the maximum frequency peak (f_{max}) in Hertz units.

$$\tau = \frac{1}{2\pi f_{max}}, \quad (1)$$

Solar simulator test using ABET Technology equipped with Source meter model 2400 Keithley that simulates sunlight to test the performance of photovoltaic devices, such as solar cells. The test was conducted at a voltage range of 0 to 2 V, an irradiation area of 0.25 cm^2, and a light intensity of 100 mW/cm^2. The efficiency of converting light energy into electricity (η) and the fill factor in DSSC (FF) can be calculated using Equations (2), where J_{SC} is the current density (mA/cm^2), V_{OC} is the open circuit voltage (Volt), and P_{in} is the light power received from the light source (solar simulator).

$$\eta = \frac{J_{SC} \times V_{OC} \times FF}{P_{in}} \times 100\%, \quad (2)$$

3. Result and Discussion

3.1 Analysis of phase

The XRD test produced data with diffraction peaks on ZnO samples, both with and without Cu doping (ZnO-Cu) at concentrations of 1%, 3%, 5%, and 10%, as shown in Figure 1(a). The sample had diffraction peaks at two theta angles, namely 31.73, 34.42, 36.23, 47.53, 56.52, 62.84, 66.30, 67.88, and 69.05°. Each of these diffraction peaks indicates the wurtzite phase with the orientation of the crystal planes in sequence at (100), (002), (101), (102), (110), (103), (200), (112), and (201). The highest intensity at an angle of 36.23° (101) indicates that the ZnO and ZnO-Cu samples have formed a single phase, according to the Joint Committee on Powder Diffraction Standards (JCPDS) card number 36-1451. Previous studies reported that the maximum peak intensity of the wurtzite phase occurs at an angle of 36.32°, corresponding to the orientation of the crystal planes (101) [17].

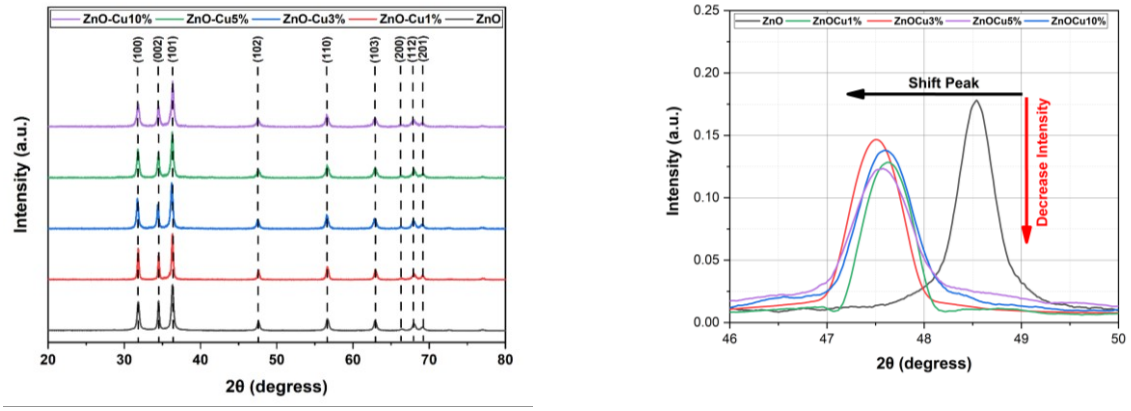

(a) (b)

Fig.1. (a) Diffraction patterning of Cu doped and undoped ZnO samples, (b) Shift lattice diffraction pattern of the ZnO samples doping Cu

Adding Cu doping to the ZnO sample reduces the intensity and shifts the angle of the diffraction peaks, as seen in Figure 1(b). At angles 31.73, 34.42, 36.23, 47.53, 56.52, 62.84, 66.30, 67.88, and 69.05°, there is an angular shift to 30.76, 33.48, 35.25, 46.60, 55.59, 61.91, 65.37, 67.01, and 68.14° after the addition of Cu doping. This change is due to the replacement of Zn^{2+} ions by Cu^{2+} ions at the ZnO site, where it is known that the radii of the Zn^{2+} and Cu^{2+} ions are similar, namely 0.74 Å and 0.73Å. The addition of doping Cu can also reduce the crystallite size in ZnO samples and even increase the number of electrons and the rate of electron movement in the conduction band [14]. The crystallite size of ZnO samples without Cu doping was 28.64 nm, whilst ZnO samples with Cu doping concentrations of 1%, 3%, 5%, and 10% are 22.52 nm, 22.27 nm, 19.65 nm, and 18.86 nm, respectively, calculated using the Debye-Scherrer formula. The smaller crystallite size in the Cu-doped ZnO sample is caused by lattice deformation and increased defect density, possibly due to strain from ion substitution [21]. Additionally, the presence of copper as a dopant can put stress on the doped samples [11].

3.2 Analysis of morphology and particle size

The morphology of the ZnO sample in this study, with a magnification of 30,000 times, shows a spherical shape with nanocrystallite oligomerization, as seen in Figure 2(a). Increasing the concentration of Cu doping in the ZnO sample, as seen in Figure 2(b-e), shows changes in shape and morphology. That is due to substituting Cu^{2+} ions into Zn sites. At a magnification of 35,000 times, the morphology of the Cu-doped ZnO sample shows a mixture of spherical and rod-shaped grains, as seen in Figure 2(b-e).

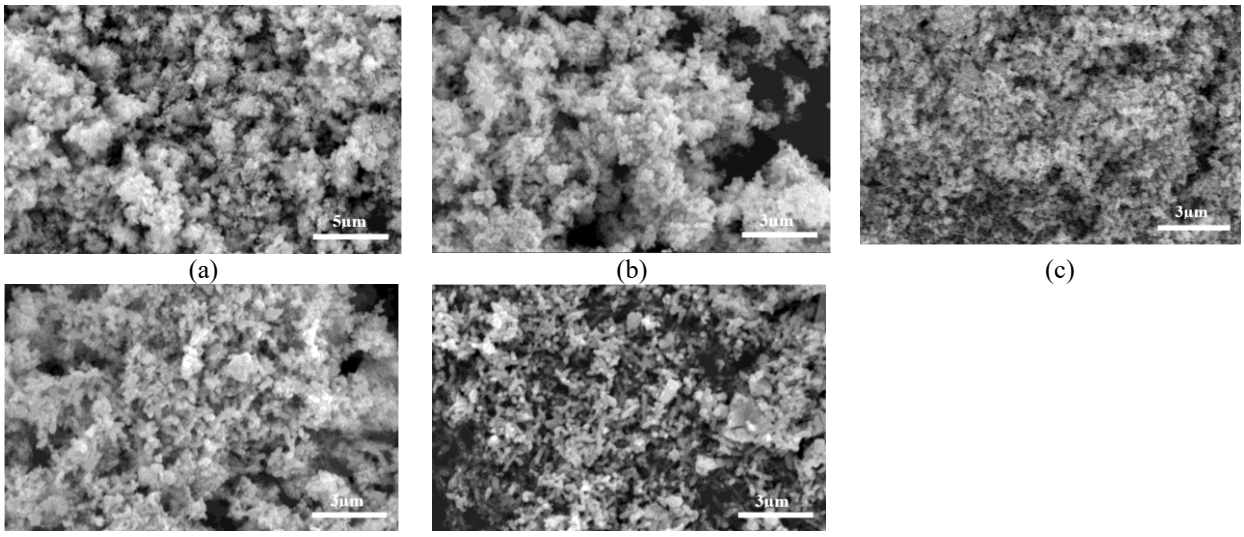

Fig.2. Morphology of samples (a) ZnO, (b) ZnO with 1% Cu doping, (c) ZnO with 3% Cu doping, (d) ZnO with 5% Cu doping, and (e) ZnO with doping 10%

The particle size distribution can be calculated using ImageJ software, the results are shown in Figure 3. Based on Figure 3, the particle size distribution for the ZnO sample without doping is 87.49 nm, while for the ZnO sample with Cu doping at concentrations of 1, 3, 5, and 10%, it is 77.77, 62.75, 59.42, and 57.80 nm, respectively.

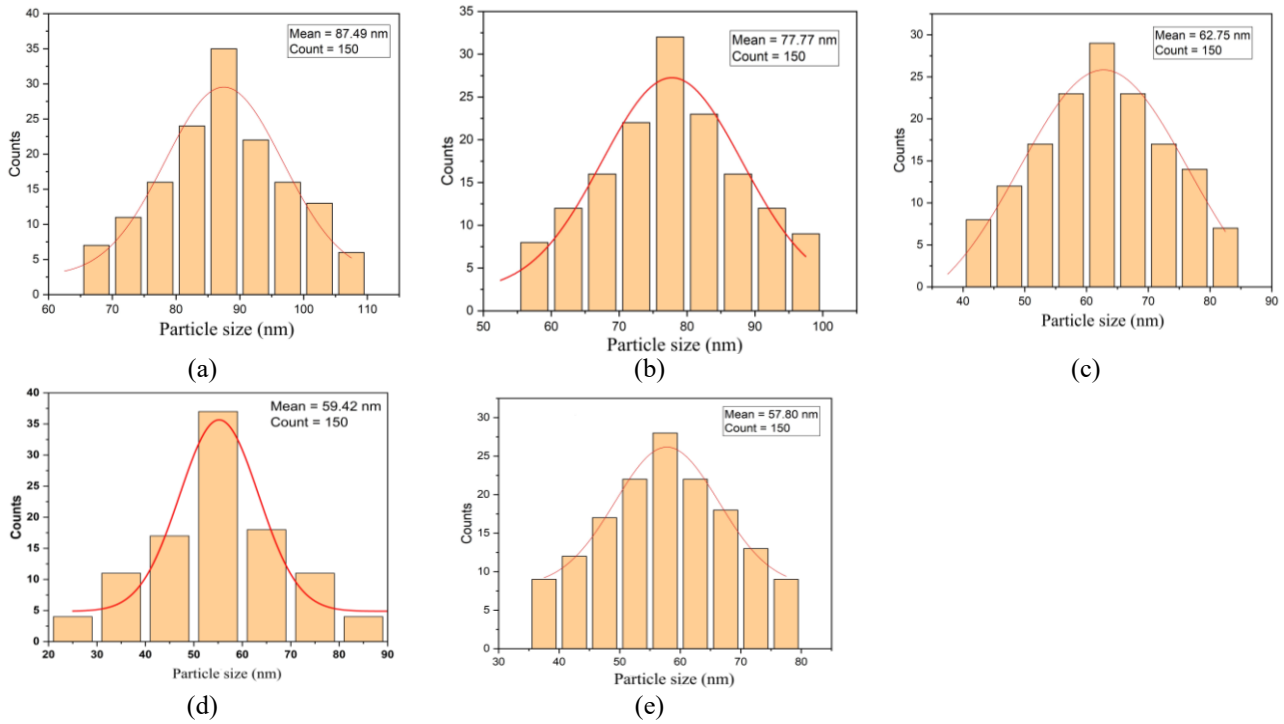

Fig.3. Particle size distribution of the sample (a) ZnO, (b) ZnO with 1% Cu doping, (c) ZnO with 3% Cu doping, (d) ZnO with 5% Cu doping, and (e) ZnO with doping Cu 10%

The difference in particle size in the ZnO sample without and with the addition of doping, which appears smaller, is due to the exchange of Cu^{2+} and Zn^{2+} ions in the ZnO lattice, and this is synchronous with the smaller crystallite size of the ZnO sample after being doped with Cu, thus affecting the efficiency of DSSC performance. Ge et al. [13] reported that a small particle is associated with a large surface area. So, it has the potential to increase the performance of DSSC, where the electrode absorbs more dye solution, which strengthens the light scattering.

3.3 Absorption UV-Vis and bandgap energy analysis

The peak of the UV-Vis absorption spectrum in Figure 4(a) for the ZnO sample is at a wavelength of 358 nm. However, with Cu doping in the ZnO sample, the absorption peak shifts to 368, 369, 370, and 372 nm for concentrations of 1, 3, 5, and 10%. The change in the absorption peak from blue-shifted to red-shifted is caused by the increasing concentration of Cu doping in the ZnO sample, resulting in changes in the electronic structure, namely the broadening of optical absorption in the ultraviolet region. Figure 4(b) shows the UV-vis spectrum at wavelengths from 400 to 700 nm for the dye solution from black mulberry fruit extract and moringa leaves, with two absorption peaks at 536 nm and 663 nm. According to previous studies, anthocyanin compounds have a wavelength absorption peak of around 450-600 nm [4], while chlorophyll pigments are found at wavelengths of 431-680 nm [22]. Mixing dyes containing anthocyanins and chlorophyll causes a bathochromic shift, also known as a red shift, so that the absorption peak of the mixed dye shifts to a longer wavelength [22]. Thus, the dye solution from this study can be used as a photosensitizer for DSSC. Because it has light absorption in the visible spectrum, even a mixture of dyes from chlorophyll and anthocyanin can increase absorption and expand the light absorption range [23].

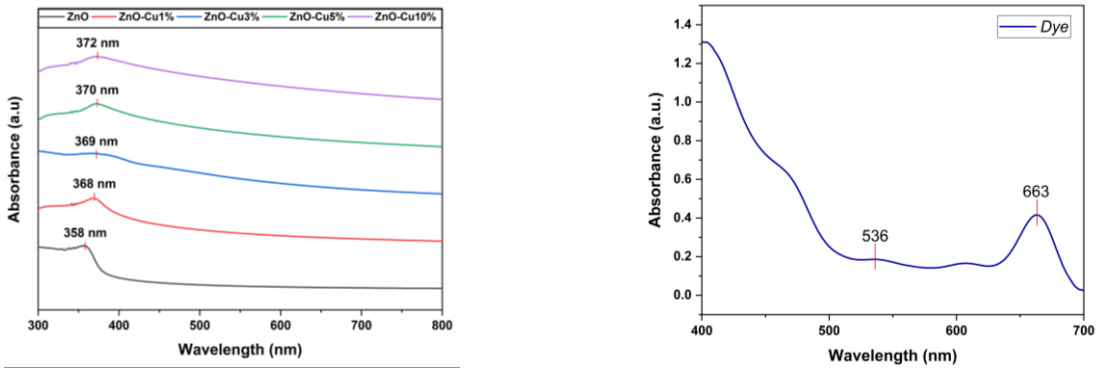

(a) (b)

Fig.4. UV-vis spectrum of samples (a) ZnO and ZnO-Cu, (b) natural dye solution

In this study, the bandgap energy for ZnO samples, both undoped and doped with Cu, can be determined from Tauc plot analysis, as shown in Figure 5(a). The ZnO sample and Cu doped ZnO 1%, 3%, 5%, and 10% have bandgap energies of 3.26, 3.00, 2.92, 2.82, and 2.59 eV, respectively. The decrease in band gap energy due to doping causes a shift in the red absorption edge, which can increase the electron mobility rate and reduce the recombination of charge carriers [24].

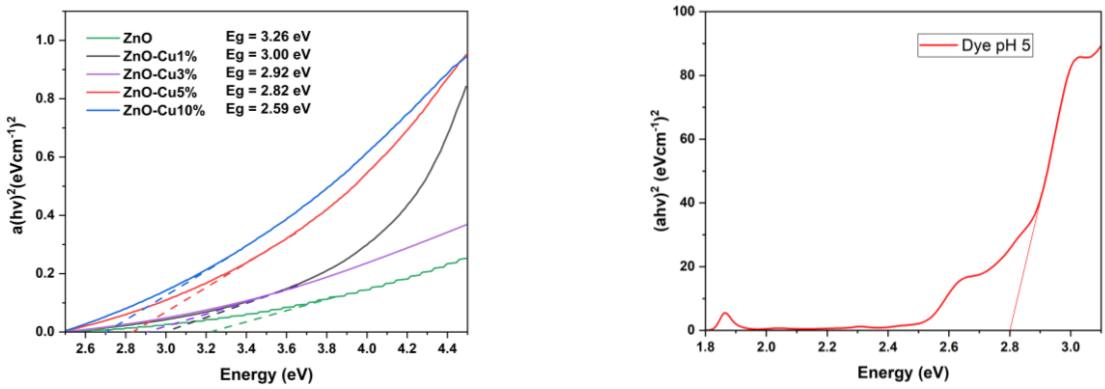

(a) (b)

Fig.5. Bandgap energy of (a) ZnO and ZnO-Cu samples, (b) natural dye solution

Figure 5(b) shows that the bandgap energy of the dye solution from black mulberry fruit extract and moringa leaves is 2.8 eV. Combining anthocyanins and chlorophyll from these plant extracts can produce a broader absorption spectrum, allowing more energy absorption from sunlight. This wider absorption wavelength can reduce the energy required for electron excitation to the conduction band, allowing the mixture of two dyes in this study to increase the photosensitizer's absorbance coefficient.

3.4 Performance DSSC

EIS measurements in dark conditions were carried out on the DSSC prototype with photoanode, counter electrode, and electrolyte to detect the possibility of electrochemical processes, especially in the charge transport process that occurs in the DSSC. The EIS test results are a Nyquist graph and a Bode phase plot, shown in Figure 6. The first semicircle (R_{ct}-CE) in the Figure 6(a) represents the charge transfer resistance at the counter electrode/electrolyte interface. In contrast, the second semicircle (R_{ct}-photoanode) describes the recombination resistance at the photoanode/electrolyte interface.

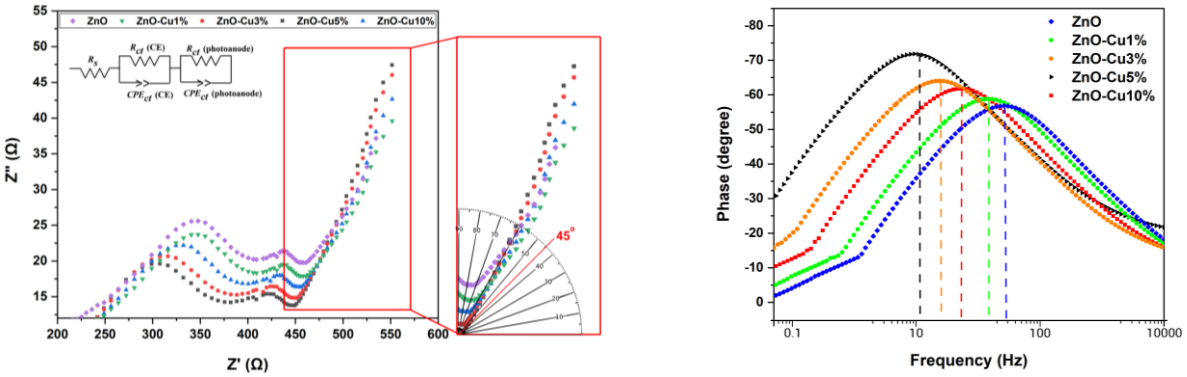

(a) (b)

Fig.6. (a) Nyquist curve, (b) Bode plot phase of ZnO nanoparticles doped Cu photoanodes

The shape of the Nyquist curve in DSSCs consists of three semicircles located in the low, mid, and high-frequency regions. In the mid-frequency range, a slope exceeding 45° (a specific angle) in the curve indicates the Warburg diffusion resistance related to the diffusion of charge carriers in the electrode material. This Warburg diffusion is an essential factor in the performance of electrochemical cells because it involves the movement of ions or molecules in the electrolyte, which shows the balance between resistance and reactance in DSSCs. This balance indicates good system stability, which can optimize the conversion of sunlight energy into electricity in solar cells. In the future, the R_s value will indicate the series resistance value associated with the system's external circuit. Electrodes with R_s values lower than the semicircle (R_{ct}) have better electrochemical energy storage performance. The DSSC on the ZnO photoanode has the largest giant semicircular shape compared to the ZnO photoanode doped with Cu. It indicates a less efficient electron transfer process because the resistance to electron flow is quite significant, thus reducing system performance and energy conversion efficiency in solar cells.

However, with the addition of Cu doping to the ZnO photoanode, the R_{ct} resistance value becomes lower, as seen in 5% Cu doping, which has a minor semicircular shape among 1%, 3%, and 10% Cu doping, which indicates that a lower of the resistance to electron transfer, so that the electron mobility is high [13]. Figure 6(b) shows the Bode phase plot curve, where the frequency peak shifts to a lower value with Cu doping on the ZnO photoanode. It shows that the charge carrier recombination rate decreases with Cu doping, allowing more light energy to be converted into electrical energy and increasing photoconversion efficiency. Cu doping at 5% has a lower frequency peak than doping at 1%, 3%, and 10%. The lifetime value of charge carriers is also an essential aspect of a solar cell's performance.

The lifetime of electrons in the cell system (τ) can be determined from the Bode phase plot curve using Equation (1), with the results presented in Table 1. Table 1 shows a significant difference in the electron lifetime in DSSCs of doped and undoped Cu photoanodes. The smaller the maximum frequency (f_{max}), the longer the electron lifetime (τ). Undoped and Cu-doped ZnO photoanodes with concentrations of 1%, 3%, 5%, and 10% have f_{max} of 74.25, 65.14, 25.74, 12.31, and 36.23 Hz, respectively, with electron lifetimes of 2.1, 2.4, 6.1, 12, and 3.6 ms.

Table 1. EIS parameters of research results of DSSC photoanodes

Photoanode Types	R_s (Ω)	R_{ct} (Ω)		f_{max} (Hz)	τ (ms)
		CE	Photoanode		
ZnO	1.11 ± 0.29	7.29 ± 0.15	4.63 ± 0.50	74.25	2.1
ZnO-Cu 1%	0.97 ± 0.27	7.01 ± 0.16	4.28 ± 0.54	65.14	2.4
ZnO-Cu 3%	0.79 ± 0.44	6.23 ± 0.14	3.98 ± 0.49	25.74	6.1
ZnO-Cu 5%	0.70 ± 0.26	5.52 ± 0.18	3.86 ± 0.53	12.31	12
ZnO-Cu 10%	0.85 ± 0.21	6.36 ± 0.26	4 ± 0.41	36.23	3.6

A high τ value indicates a longer lifetime of electrons generated by photons in the cell, meaning that electrons survive longer before being trapped or returning to the ground state, allowing more electrons to contribute to generating an electric current. Increasing the concentration of Cu doping in the ZnO photoanode can increase the efficiency of the DSSC. However, the performance efficiency of the DSSC doped with 10% Cu decreased. It can be seen from the increase in the R_{ct} values on the photoanode and counter electrode (CE) and the electron lifetime, which were 6.36 Ω, 4 Ω, and 3.6 ms, respectively. Cu doping with a high concentration (10%) has the potential to create more trap states in the ZnO semiconductor, thus limiting the number of free electrons that can move. As a result, the flow of electrons is reduced, impacting the DSSC's performance and reducing its efficiency. Cu doping in the DSSC photoanode improves its electrochemical performance in energy conversion compared to the ZnO photoanode alone. Ge et al. [13] in their research reported that ZnO photoanodes with 1% Cu doping, produced through the hydrothermal method, have an electron lifetime of 1.06 ms, which is lower than that of research carried out using the green synthesis method for producing Cu-doped ZnO photoanodes. It has been proven that 1% Cu-doped ZnO in this work has an electron lifetime of 2.4 ms. Even the electrochemical performance of ZnO photoanodes without Cu doping in this study was also better, at 2.1 ms, compared to ZnO prepared through the coprecipitation method (1.96 ms) [25] and commercial ZnO (1.32 ms) [13]. It shows that synthesizing ZnO nanoparticles using the green synthesis pathway improves electrochemical performance in DSSC.

The solar simulator test can evaluate the efficiency (η) of DSSC performance, which reflects its ability to convert sunlight into electrical energy. The results showing the relationship between voltage (V) and current density (J_{SC}) are presented in Figure 7. The figure allows further analysis of the DSSC performance efficiency, which is given in Table 2. The ZnO-Cu5% DSSC photoanode shows the highest short-circuit current (J_{SC}) of 1.11 mA/cm^2, while the open-circuit voltage (V_{OC}) of all samples is almost the same due to the very similar structure, chemical reactivity, and optical properties between Cu^{2+} and Zn^{2+} ions [11].

The DSSC efficiency value on the ZnO-Cu5% photoanode is 1.67%, higher than that of ZnO-Cu10%, which is 1.48%. The excessive influx of Cu ions into ZnO causes a decrease in the effectiveness of the transition process and electron transfer in the DSSC [13].

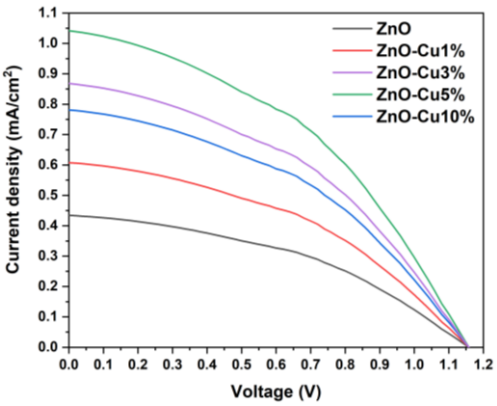

Fig.7. J-V curve of DSSC with ZnO doped Cu photoanode

The efficiency of DSSC with Cu-doped ZnO photoanode synthesized through green synthesis using pineapple peel extract has a higher energy conversion efficiency in DSSC than the results of several previous researchers, as shown in Table 3.

Table 2. DSSC photovoltaic performance with photoanodes and dye solution

Photoanoda	J_{SC} (mA/cm^2)	V_{OC} (Volt)	FF	η (%)
ZnO	0.46 ± 0.03	1.14 ± 0.05	0.23 ± 0.01	0.48 ± 0.04
ZnO-Cu1%	0.65 ± 0.04	1.14 ± 0.05	0.32 ± 0.01	0.95 ± 0.01
ZnO-Cu3%	0.84 ± 0.05	1.14 ± 0.05	0.42 ± 0.02	1.60 ± 0.01
ZnO-Cu5%	1.11 ± 0.08	1.14 ± 0.05	0.33 ± 0.02	1.67 ± 0.01
ZnO-Cu10%	0.93 ± 0.07	1.14 ± 0.05	0.35 ± 0.01	1.48 ± 0.02

Table 3. The efficiency of Cu doped ZnO based DSSCs from green synthesis results compared with previous research results

Synthesis Method	Photoanode Type	Dye	DSSC Efficiency, η (%)	References
Sequential Ion Layer Adsorption and Reaction (SILAR)	ZnO-Cu 1%	Hypericum perforatum L. flowers	0.42	[2]
co-precipitation	ZnO-Cu 3%, ZnO-Cu 5%	N3	1.34, 1.09	[26]
co-precipitation	ZnO-Cu 5%	N719	0.34	[8]
co-precipitation	ZnO-Cu 5%	N3	1.09	[26]
Radio Frequency (RF) sputtering in room temperature	ZnO, ZnO-Cu	$H_2PtCl_6.6H_2O$ in 2-propanol .	0.16, 0.56	[27]
Layered Double Hydroxide (LDH)	ZnO-Cu 1%	D149	0.83	[13]
sol-gel	ZnO-Cu 5%	Xanthene	0.78	[14]
Green synthesis	ZnO, ZnO-Cu 1%, ZnO-Cu 5%	Moringa leaves and black mulberry fruit	0.48, 0.95, 1.67	This work

Cu-doped ZnO photoanodes from various methods that several researchers have reported, as in Table 3, show different DSSC efficiency values. ZnO photoanodes without and with Cu doping, from the results of synthesis through the green synthesis method in this study, showed better DSSC performance, where the efficiency value was higher than the results of previous studies. In addition, dye solutions from natural materials, namely black mulberry extract, and moringa leaves, also play an essential role as sensitizers in absorbing photons, so they can be used to replace synthetic sensitizer dyes.

4. Conclusion

In this study, the ZnO nanoparticles doped with Cu were well synthesized using bioreduction from pineapple peel extract with the green synthesis method. This sample has a wurtzite phase with a nanocrystallite size. Increasing the concentration of Cu doping in ZnO samples can cause a decrease in the bandgap energy value, where it is known that the bandgap before Cu doping is 3.26 eV, and after Cu doping is 3, 2.92, 2.82, and 2.59 eV for doping concentrations of 1, 3, 5, and 10%. Combining anthocyanin and chlorophyll from black mulberry fruit extract and moringa leaves produces a broader absorption spectrum at 536 and 663 nm, with a bandgap of 2.8 eV. Cu-doped ZnO photoanode increases the performance efficiency of DSSC, as evidenced by the results of electrochemical tests, where the electron lifetime for the ZnO photoanode without doping is 2.1 ms. Conversely, ZnO photoanodes doped with Cu at concentrations of 1%, 3%, 5%, and 10% had electron lifetimes of 2.4 ms, 6.1 ms, 12 ms, and 3.6 ms, respectively. Cu doping at a concentration of 5% on the ZnO photoanode provided an efficiency DSSC of 1.67%, higher than that of the ZnO photoanode without doping (0.48%) and with Cu doping at concentrations of 1% (0.95%), 3% (1.6%) and 10% (1.48%). Thus, a Cu-doped ZnO photoanode synthesized by the green route shows good electrochemical performance.

Conflict of interest statement

The authors declare that they have no conflict of interest in relation to this research, whether financial, personal, authorship or otherwise, that could affect the research and its results presented in this paper.

CRediT author statement

Rohmawati, L.: Conceptualization, Methodology, Investigation, Writing-Original Draft; **Ferdianto, S.P.**: Methodology, Investigation, Software; M Samsul M.: Methodology, Software; Fadhil F.A.: Methodology, Software; Fariz I.M.: Methodology, Software; **Setyarsih, W.**: Conceptualization, Methodology, Writing-Original Draft; **Supardi, Z.A.I.**: Conceptualization, Writing-Original Draft; **Darminto, D.**: Conceptualization, Writing-Original Draft.
The final manuscript was read and approved by all authors.

Acknowledgements

This research can be completed according to the author's expectations thanks to the assistance of various parties, mainly from institutions that have supported the implementation of this research.
The authors would like to thank the Director Riset Teknologi and Pengabdian Masyarakat (DRTPM) of the Kementerian Pendidikan, Kebudayaan, Riset, dan Teknologi for the funds provided through research on the Regular Fundamental scheme with the Decree of the Rector of Universitas Negeri Surabaya, Number 841/UN38/HK/2024.

References

1 Neikov O.D., Naboychenko S.S., Murashova I.B. (2019) Production of rare metal powders. *Handbook of Non-Ferrous Metal Powders (Second Edition)*, Chapter 24, 757-829. https://doi.org/10.1016/B978-0-08-1005439.00024-5.

2 Göde F., Balpinar N. (2023) Dye-sensitized solar cells fabricated using ZnO:Cu thin films and dye extracted from Hypericum perforatum L. flowers. *Dig. J. Nanomater. Biostruct*. 18(1), 389-402. https://doi.org/10.15251/DJNB.2023.181.389.

3 Huo J., Ni Y., Li D., Qiao J., Huang D., Sui X., Zhang Y. (2023) Comprehensive structural analysis of polyphenols and their enzymatic inhibition activities and antioxidant capacity of black mulberry (*Morus nigra L.*). *Food Chem*., 427, 136605. https://doi.org/10.1016/j.foodchem.2023.136605.

4 Yildiz Z.K., Atilgan A., Atli A., Özel K., Altinkaya C., Yildiz A. (2019) Enhancement of efficiency of natural and organic dye sensitized solar cells using thin film TiO_2 photoanodes fabricated by spin-coating. *J. Photochem. Photobiol. A Chem*., 368, 23-29. https://doi.org/10.1016/j.jphotochem.2018.09.018.

5 Rotulung J.C., Djarkasi G.S.S., Taroreh M.I.R. (2023) Pengaruh Penambahan Sari Daun Kelor Terhadap Kadar Kalsium Dan Sifat Sensoris Pada Susu Kenari. *Jurnal Teknologi Pertanian*., 14(2), 110-118. https://doi.org/ https://doi.org/10.35791/jteta.v14i2.51877

6 Fajri, Rahmatu R., Alam N. (2018) Kadar Klorofil Dan Vitamin C Daun Kelor (Moringa Oleifera Lam) dari Berbagai Ketinggian Tempat Tumbuh. *AGROTEKBIS: Jurnal Ilmu Pertanian*., 6(2), 152-158. Available at: http://jurnal.faperta.untad.ac.id/index.php/agrotekbis/article/view/270/263

7 Vaiano V., Matarangolo M., Murcia J.J., Rojas H., Navío J.A., Hidalgo M.C. (2018) Enhanced photocatalytic removal of phenol from aqueous solutions using ZnO modified with Ag. *Appl. Catal. B*, 225, 197-206. https://doi.org/10.1016/j.apcatb.2017.11.075.

8 Das A., Nair R.G. (2020) Effect of aspect ratio on photocatalytic performance of hexagonal ZnO nanorods. *J. Alloys Compd*., 817: 153277. https://doi.org/10.1016/j.jallcom.2019.153277.

9 Wu D., Wang Y., Ma N., Cao K., Zhang W., Chen J., Wang D., Gao Z., Xu F., Jiang K. (2019) Single-crystal-like ZnO mesoporous spheres derived from metal organic framework delivering high electron mobility for enhanced energy conversion and storage performances. *Electrochim. Acta*, 305, 474–483. https://doi.org/10.1016/j.electacta.2019.0

10 Kuang M., Zhang J., Wang W., Chen J., Liu R., Xie S., Wang J., Ji Z. (2019) Synthesis of octahedral-like $ZnO/ZnFe_2O_4$ heterojunction photocatalysts with superior photocatalytic activity. *Solid State Sci*., 96, 105901. https://doi.org/10.1016/j.solidstatesciences.2019.05.012.

11 Esgin H., Caglar Y., Caglar M. (2022) Photovoltaic performance & physical characterization of Cu doped ZnO nanopowders as photoanode for DSSC. *J.Alloys Compd*., 890, 161848. https://doi.org/10.1016/j.jallcom.2021.16184 8

12 Gaurav A., Beura R., Kumar J.S., Thangadurai P. (2019) Study on the effect of copper ion doping in zinc oxide nanomaterials for photocatalytic applications. *Mater. Chem. Phys*., 230, 162-171. https://doi.org/10.1016/j.matchemphys.2019.03.056.

13 Ge Z., Wang C., Chen T., Chen Z., Wang T., Guo L., Qi G., Liu J. (2021) Preparation of Cu-doped ZnO nanoparticles via layered double hydroxide and application for dye-sensitized solar cells. *J. Phys. Chem. Solids*, 150. https://doi.org/10.1016/j.jpcs.2020.109833.

14 Kumbhar D., Kumbhar S.S., Delekar S., Nalawade R., Nalawade A. (2019) Photoelectrochemical cell performance cu doped zno photoanode sensitized by xanthene dyes. *Nanosyst: Phys. Chem. Math*., 10(4), 466–474. http://doi.org/10.17586/2220-8054-2019-10-4-466-474.

15 Muthuvel A., Jothibas M., Manoharan C. (2020) Effect of chemically synthesis compared to biosynthesized ZnO-NPs using *Solanum nigrum* leaf extract and their photocatalytic, antibacterial and invitro antioxidant activity. *J. Environ. Chem. Eng.,* 8, 103705. https://doi.org/10.1016/j.jece.2020.103705.

16 Kazemi S., Hosseingholian A., Gohari S.D., Feirahi F., Moammeri F., Mesbahian G., Moghaddam Z.S., Ren Q. (2023) Recent advances in green synthesized nanoparticles: from production to application. *Mater. Today Sustain*., 24, 100500. https://doi.org/10.1016/j.mtsust.2023.100500.

17 Khan M.M., Harunsani M.H., Tan A.L., Hojamberdiev M., Poi Y.A., Ahmad N. (2020) Antibacterial Studies of ZnO and Cu-Doped ZnO Nanoparticles Synthesized Using Aqueous Leaf Extract of *Stachytarpheta jamaicensis*. *BioNanoScience*, 10(4), 1037–48. https://doi.org/10.1007/s12668-020-00775-5.

18 Rohmawati L., Lailia L.R., Putri N.P., Nasir M., Darminto D. (2024) Characterization of ZnO Nanoparticles Pineapple Skin Extract (*Ananas comosus L.*) as Photocatalytic Activity. *J. Water Environ. Nanotechnol*., 9(1), 112–123. http://doi.org/10.22090/jwent.2024.01.08.

19 Gaur J., Vikrant K., Him K.H., Kumar S., Pal M., Badru R., Masand S., Momoh J. (2023) Photocatalytic degradation of Congo red dye using zinc oxide nanoparticles prepared using Carica papaya leaf extract. *Mater. Today Sustain*., 22, 100339. https://doi.org/10.1016/j.mtsust.2023.100339.

20 Andari R. (2020) Distance Variation of Light Source Effects toward Dye Sensitized Solar Cell (DSSC) Performance using Anthocyanin Extract from Rosella Flower. *JPSE (Journal of Physics Science and Engineering),* 5(1), 31–35. http://doi.org/10.17977/um024v5i12020p031.

21 Nazim V.S., El-Sayed G.M., Amer S.M., Nadim A.H. (2023) Optimization of metal dopant effect on ZnO nanoparticles for enhanced visible LED photocatalytic degradation of citalopram: comparative study and application to pharmaceutical cleaning validation. *Sustain. Environ. Res*., 33(39), 1-16. https://doi.org/10.1186/s42834-023-00198-3.

22 Munandar M.R., Hakim A.S.R., Puspitadindha H.A., Andiyani S.P., Nurosyid F. (2022) The effect of mixing Chlorophyll-Antocyanin as a natural source dye on the efficiency of dye-sensitized solar cell (DSSC). *J. Phys. Conf. Ser*., 2190(1), 012042. https://doi.org/10.1088/1742-6596/2190/1/012042.

23 Sakshi, Singh P.K., Shukla V.K. (2022) Widening spectral range of absorption using natural dyes: Applications in dye sensitized solar cell. *Mater. Today Proc*., 49(8), 3235-3238. https://doi.org/10.1016/j.matpr.2020.12.287.

24 Kyaw K.K., Toe H. (2020) Characterization and Doping Effect of Cu-Doped ZnO Films. *Mater. Sci. Eng. A,* 10(3-4), 43-52. https://doi.org/10.17265/2161-6213/2020.3-4.001.

25 Ramya M., Nideep T.K., Nampoori V.P.N., Kailasnath M. (2021) The impact of ZnO nanoparticle size on the performance of photoanodes in DSSC and QDSSC: a comparative study. *J Mater Sci: Mater Electron*., 32, 3167-3179. https://doi.org/10.1007/s10854-020-05065-0.

26 Rajan A.K., Louis C. (2020) Localized surface plasmon resonance of Cu-doped ZnO nanostructures and the material's integration in dye sensitized solar cells (DSSCs) enabling high open-circuit potentials. *Journal of Alloys and Compounds,* 829, 154497. https://doi.org/10.1016/j.jallcom.2020.154497.

27 Alam M.W., Ansari M.Z., Aamir M., Waheed-Ur-Rehman M., Parveen N., Ansari S.A. (2022) Preparation and Characterization of Cu and Al Doped ZnO Thin Films for Solar Cell Applications. *Crystals*, 12, 128. https://doi.org/10.3390/cryst12020128.

AUTHORS' INFORMATION

Rohmawati, Lydia – Master (Sci.), Lecturer in Department of Physics, Faculty of Mathematic and Sciences, Universitas Negeri Surabaya, Surabaya, Indonesia; Scopus Author ID: 57201676108; https://orcid.org/0000-0002-0047-3487; lydiarohmawati@unesa.ac.id

Ferdianto, Sandy Prayoga – Bachelor(Sci.), Department of Physics, Faculty of Mathematic and Sciences, Universitas Negeri Surabaya, Surabaya, Indonesia; Scopus Author ID: 59483385500; https://orcid.org/0009-0004-1530-6421; sandy.20026@mhs.unesa.ac.id

Ma'arif, M Samsul – Bachelor(Sci.), Department of Physics, Faculty of Mathematic and Sciences, Universitas Negeri Surabaya, Surabaya, Indonesia; Scopus Author ID: 59484056700; https://orcid.org/0009-0003-6442-4793; msamsul.20038@mhs.unesa.ac.id

Ardiansyah, Fadhil Figo – Bachelor(Sci.), Department of Physics, Faculty of Mathematic and Sciences, Universitas Negeri Surabaya, Surabaya, Indonesia; Scopus Author ID: 59483930300; https://orcid.org/0009-0004-9974-5949; fadhil.20027@mhs.unesa.ac.id

Muadhif, Fariz Irkham – M.Sc Student,- Post graduate student, Department of Nanotechnology, Institut Teknologi Bandung, Bandung; Researcher in the Research Center for System Nanotechnology, National Research and Innovation Agency (BRIN),

Tangerang Selatan, Indonesia; Scopus Author ID: 58821604300; https://orchid.org/0009-0004-7357-2912; 28723005@mahasiswa.itb.ac.id

Setyarsih, Woro – Master (Sci.), Lecturer in Department of Physics, Universitas Negeri Surabaya, Surabaya, Indonesia. Scopus Author ID: 57193132412; https://orcid.org/0000-0001-8344-2768; worosetyarsih@unesa.ac.id

Supardi, Zainul Arifin Imam – Ph.D, Lecturer in Department of Physics, Universitas Negeri Surabaya, Surabaya, Indonesia. Scopus Author ID: 6508147948; https://orcid.org/0000-0002-9150-6378; zainularifin@unesa.ac.id

Darminto, Darminto – Ph.D, Professor, Lecturer in Department of Physics, Institut Teknologi Sepuluh Nopember, Surabaya, Indonesia. Scopus Author ID: 6602346156; https://orcid.org/0000-0002-6269-9246; darminto@physics.its.ac.id